Model-based estimation of individual muscle force based on measurements of muscle activity in forearm muscles during isometric tasks

Andrea Zonnino *Student Member, IEEE* and Fabrizio Sergi, *Member, IEEE*,

***Abstract*—Objective: Several forward dynamics estimation approaches have been proposed to estimate individual muscle force. However, characterization of the estimation error that arises when measurements are available only from a subset of the muscles involved in the movement under analysis, as it is the case of the forearm muscles, has been limited. Our objectives were: 1) to quantify the accuracy of forward-dynamics muscle force estimators for forearm muscles; 2) to develop a muscle force estimator that is accurate even when measurements are available only from a subset of muscles acting on a given joint or segment.**

Methods: We developed a neuromusculoskeletal (NMSK) estimator that integrates forward dynamics estimation with a neural model of muscle co-contraction to estimate individual muscle force during isometric contractions, suitable to operate when measurements are not available for all muscles. We developed a computational framework to assess the effect of physiological variability in muscle co-contraction, cross-talk, and measurement error on the estimator accuracy using a sensitivity analysis. We thus compared the performance of our estimator with the performance of a standard estimator that neglects the contribution of unmeasured muscles.

Results: The NMSK estimator reduces the estimation error by 25% in average noise conditions. Moreover, the NMSK estimator is robust against physiological variability in muscle co-contraction and outperforms the standard estimator even when the validity of the neural model is compromised.

Conclusion and Significance: In isometric tasks, the NMSK estimator reduces muscle force estimation error compared to a standard estimator, and may enable future applications involving estimation of forearm muscle force during coordinated movements.

***Index Terms*—muscle force estimation, forward dynamics estimation, surface EMG, wrist biomechanics**

I. Introduction

It is currently not possible to non-invasively measure individual muscle forces from a complete set of muscles *in-vivo* during tasks that require coordinated muscle co-activation using non invasive protocols. Developing a technique capable of overcoming this limitation would represent one of the biggest breakthrough in biomechanics [1]. Such technique will in fact give fundamental contributions both to answer many open questions in basic neuromuscular physiology, motor control and biomechanics and to obtain clinically relevant insights in neurorehabilitation, orthopedics and gait analysis. For instance, in motor disorders, such as cerebral palsy, or stroke, the possibility to determine how an external load is shared between muscles would enable to directly identify the set of muscles responsible for the abnormal activity thus allowing more focused interventions. Similarly, in athletes with recurring muscular and articular injuries, such a technique would enable the examination of how the central nervous system solves muscle redundancy and adapts the selection of the contraction strategy in presence of fatigue or injuries. In this way it would be possible to determine the role of each muscle in the evolution of the injury.

Non-invasive approaches have been proposed to estimate individual muscle force using estimation techniques [2], [3]. These methods rely on the evidence that muscle forces produce joint movement and torque. However, since neither joint position nor joint torque provide information at the individual muscle level, these measurements need to be augmented via estimators to quantify forces at the individual muscle level.

Current estimation algorithms can be grouped in two macro-categories: inverse and forward dynamics approaches. Inverse dynamics estimators use either the measured joint torque or joint angle to estimate the contribution of different muscles to the measured movement [4]–[7]. Cost-function minimization is usually employed to address muscle redundancy [8]; unfortunately, the assumption of a cost function that is generalizable across tasks and subjects does not always hold, with the estimated forces highly sensitive to the selection of such function [9], [10].

Forward dynamics estimators [11]–[18], on the contrary, make no assumption on the strategy adopted to solve the muscle redundancy. They typically require knowledge of the limb's geometry, measurements of joint torque, and measurements of muscle activity. While recently shear wave elastography has been proposed to indirectly quantify muscle activity [19]–[21], measurements of muscle activity are more commonly obtained with surface electromyography (sEMG).

However, since sEMG can only measure the activity of superficial muscles, current estimation approaches neglect the contribution from non-superficial muscles to the joint torque. This approximation might be appropriate when estimating forces from the lower limbs muscles, however it is likely to result in inaccurate estimates when applied to complex body segments that have many muscles arranged in different layers, such as the forearm muscles that control hand and wrist movements. While most of the recent research done in the area has focused on developing computationally efficient estimators

FS (corresponding author - fabs@udel.edu), AZ are with the Human Robotics Laboratory, Department of Biomedical Engineering, University of Delaware, Newark DE, 19713 USA.

We acknowledge support from the University of Delaware Research Foundation grant no. 16A01402, and from startup funds by the University of Delaware.

that could work in dynamic conditions [13], [16] or in real-time applications (e.g. brain-machine interfaces, biofeedback control loops of robotic devices) [7], [18], these studies have not addressed the problem of individual muscle force estimation. As such, it is still not clear what is the accuracy of the estimation process, even for isometric contractions, when measurements of muscle activity are not available from all muscles.

In this paper, we present a novel estimator that integrates a forward dynamics estimation approach with a neuromuscular model of muscle contraction, used to estimate the effect of unmeasured muscle activity on joint torque. We hypothesized that the novel estimator would be able to return more accurate estimates of muscle force compared to a standard musculoskeletal estimator, when both are used to estimate forces of the forearm muscles during isometric tasks involving the wrist. Since the true value of the muscle force is not measurable through *in-vivo* procedures, it would be impossible to quantify accuracy of any muscle force estimator using purely experimental protocols. As such, we chose to simulate measurements using a musculoskeletal model, which allowed to run simulations to quantify the deviation between the estimated and the assumed true values of muscle forces. We thus developed a computational framework based on a realistic musculoskeletal model [22] that simulates muscle forces and virtual measurements of muscle activity during isometric contractions. To test our hypothesis, we simulated calibration experiments aimed at estimating individual muscle force from a set of measurements of muscle activity under a set of experimental conditions, when realistic conditions of measurement noise and physiological variability are included.

A preliminary version of this work has been reported in [23].

II. Materials and Methods

A. Model

The computational framework presented in this paper is based on the upper extremity musculoskeletal model (MSM) presented by Saul et. al [22]. Only a subset of the objects in the model are used for this analysis; specifically, the upper arm is considered grounded, with motion allowed only for the forearm and hand. As such, the reduced model has four degrees of freedom (DOFs): elbow flexion/extension (eFE), pronation/supination (PS), wrist flexion/extension (FE), and wrist radio/ulnar deviation (RUD). A total of $m_{tot} = 15$ muscles have been used for actuation of the MSM (Tab. I); however, for some of the analyses presented, a further reduced set of muscles will be considered.

Each muscle included in the MSM is modeled as a Hill-type musculo-tendon (MT) unit in isometric conditions [24], [25]. For given values of muscle activation a and muscle length l_m, the musculo-tendon force f_{MT} of each MT unit is determined by:

$$f_{MT}(l_m, a) = F_{\max}(a\tilde{f}_A(l_m) + \tilde{f}_P(l_m))\cos(\alpha(l_m)) \quad (1)$$

where $F_{\max}$ is the maximum isometric muscle force, α is the muscle pennation angle, and $\tilde{f}_A$ and $\tilde{f}_P$ are the active and passive force multipliers, respectively [25]. Assuming the tendon to be inextensible [26], the length of each muscle is directly related to the posture of the wrist joint and independent from muscle activation. As such, in a given posture the MT force is linearly proportional to muscle activity.

To simulate indirect measurements of muscle activity, a linear dependence is then assumed between the value of activation a and the measurement M:

$$a = \gamma M \quad (2)$$

where γ is a muscle-specific scaling coefficient that needs to be derived via a proper calibration procedure to estimate activation and force from the measured values of M.

B. Muscle Force Estimation

In general, the relationship between muscle force and joint torque is provided by:

$$\boldsymbol{\tau} = -\mathbf{J}\mathbf{f}_{\mathbf{MT}} \quad (3)$$

As such, combining eq. (1) - (3), and using the bold notation to refer to vector or matrix quantities, a linear relationship can be derived between $\boldsymbol{\tau}$ and $\boldsymbol{M}$:

$$\boldsymbol{\tau} = -\mathbf{J}\cos(\boldsymbol{\alpha})\mathbf{F}_{\mathbf{max}}(\tilde{\mathbf{f}}_{\mathbf{A}}\mathbf{M}\boldsymbol{\gamma} + \tilde{\mathbf{f}}_{\mathbf{P}}), \quad (4)$$

where $\mathbf{J}$ is the muscular Jacobian whose component r_{ij} represents the moment arm of the muscle j with respect of the joint angle i. $\mathbf{F}_{\mathbf{max}}$, $\boldsymbol{\alpha}$, and $\tilde{\mathbf{f}}_{\mathbf{A}}$ are diagonal matrices that contain the respective scalar parameters for each muscle. $\boldsymbol{\gamma}$ and $\tilde{\mathbf{f}}_{\mathbf{P}}$ are vectors that contain the muscle-specific scaling coefficient and passive force for each muscle, respectively.

From eq. (4), it can be seen that there is a linear relationship between $\boldsymbol{\tau}$ and $\mathbf{M}$. As such, by measuring joint torque, measuring the activation of all muscles producing torque about a given joint, and accounting for the passive force of all such muscles, all elements in the vector $\boldsymbol{\gamma}$ can be estimated with a proper calibration procedure.

1) Musculoskeletal estimator (MSK): While the general description reported above is theoretically correct, the assumptions included therein are almost never achievable in practice. In fact, standard non-invasive muscle activation measurement techniques, such as sEMG, can only provide a measurement of the activation of superficial muscles. Usually, activation of $m < m_{tot}$ muscles is available using sEMG. A standard approach to calibration, in these cases, neglects the contribution of unmeasured muscles and of passive forces, simplifying eq. (4) as

$$\boldsymbol{\tau} = -\mathbf{J}\cos(\boldsymbol{\alpha})\mathbf{F}_{\mathbf{max}}\tilde{\mathbf{f}}_{\mathbf{A}}\mathbf{M}_{\mathbf{m}}\gamma_{\mathbf{m}} \quad (5)$$

where $\mathbf{M}_{\mathbf{m}}$ and $\boldsymbol{\gamma_m}$ are the subsets of $\mathbf{M}$ and $\boldsymbol{\gamma}$ that pertain to the measurable muscles.

Since eq. (5) is a linear equation of the form $\mathbf{y} = \mathbf{X}\boldsymbol{\beta}$, with proper experimental design, it is possible to define a set of n tasks, defined as a set of joint torques applied at different postures in isometric conditions, such that the resulting experimental matrix $\bar{\mathbf{X}} := [\mathbf{X_1}; \mathbf{X_2}; ...; \mathbf{X_n}]$ is of full rank. When this condition is satisfied, it is possible to estimate the vector $\boldsymbol{\beta} := \boldsymbol{\gamma}_m$ using a standard least squares fit given measurements of $\bar{\mathbf{y}} := [\boldsymbol{\tau_1}; \boldsymbol{\tau_2}; ...; \boldsymbol{\tau_n}]$.

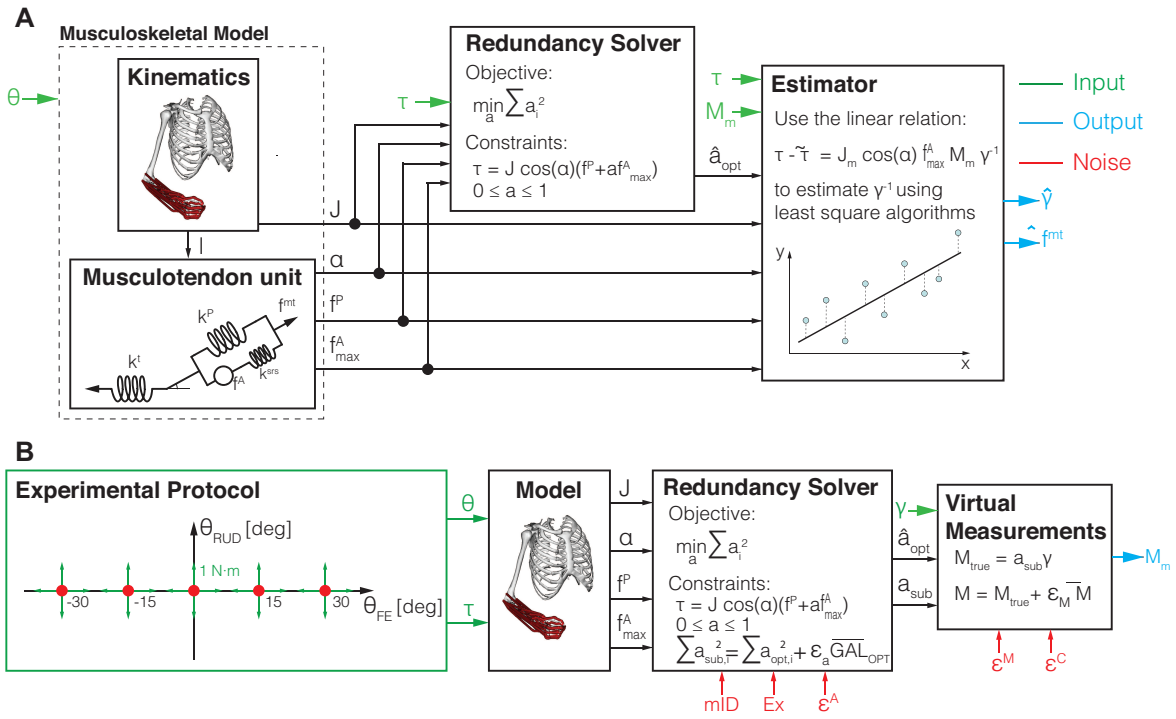

Fig. 1. A) Block diagram of the proposed estimator. (B) Block diagram of the computational framework implemented for the sensitivity analysis used to quantify the accuracy of the proposed estimator. Parameters ϵ^A, ϵ^C ϵ^M represents the level of physiological variability, cross-talk, and measurement error, respectively; m_{ID} is a vector that contains the set of measurable muscles, and Ex is a boolean variable that indicate if finger muscles are active or not.

2) Neuromusculoskeletal estimator (NMSK): We propose a novel estimation algorithm capable of dealing with cases where the approximations made within the MSK estimator do not allow sufficient accuracy, due to unmeasured muscle activations. Instead of neglecting the contribution of unmeasured muscles and of passive muscle forces, our new estimator integrates quantities available through measurements with parameters extracted from a musculoskeletal model to improve the accuracy of the estimation of vector $\boldsymbol{\gamma_m}$. The estimator extracts the contribution of unmeasured muscle forces using a neural model that provides a solution for the muscle redundancy problem. As such, we refer to our estimator as neuromusculoskeletal estimator (NMSK).

A schematic of the NMSK estimator is shown in Fig. 1A. For a generic task, defined by a specific value of joint angle and torque, static optimization is used to obtain the optimal muscle activation vector, $\hat{\mathbf{a}}_{\mathbf{opt}}$, that minimizes the Global Activation Level GAL $= \sum a_i^2$ [26]. The subset $\hat{\mathbf{a}}_{\bar{\mathbf{m}}}$ of $\hat{\mathbf{a}}_{\mathbf{opt}}$ that correspond to unmeasured muscles are then included in eq. (4), together with the model-estimated passive muscle force:

$$\begin{aligned}\boldsymbol{\tau} =& -\mathbf{J}\cos(\boldsymbol{\alpha})\mathbf{F_{max}}\tilde{\mathbf{f}}_{\mathbf{P}} - \mathbf{J}_{\bar{\mathbf{m}}}\cos(\boldsymbol{\alpha})\mathbf{F_{max}}\tilde{\mathbf{f}}_{\mathbf{A}}\hat{\mathbf{a}}_{\bar{\mathbf{m}}} \\ & -\mathbf{J}_{\mathbf{m}}\cos(\boldsymbol{\alpha})\mathbf{F_{max}}\tilde{\mathbf{f}}_{\mathbf{A}}\mathbf{M}_{\mathbf{m}}\boldsymbol{\gamma}_{\mathbf{m}}\end{aligned} \tag{6}$$

where the subcomponents of the Jacobian corresponding to measured and unmeasured muscles, $\mathbf{J_m}$ and $\mathbf{J}_{\bar{\mathbf{m}}}$ respectively, have been decoupled.

Eq. (6) shows that the measured joint torque is the compound effect of three terms: the first that represents the contribution of the passive elastic component of all muscles in the limb; the second and the third that represent, instead, the contribution of the active component of the unmeasured and measured muscles, respectively. As the tendons are assumed to be inextensible, the length of the each MT unit, and thereby the set of MT parameters, are unequivocally determined given the value of joint angle. Given a value of joint torque, then, the static optimizer will always converge to the same optimum, making the optimal muscle activation vector unequivocally related to the set of joint posture and joint angle. As such, all the parameters in the first two terms can be obtained from the neuromusculoskeletal model and are constant for a set of joint torque and posture. Thus, if we define the quantity $\tilde{\boldsymbol{\tau}} := -\mathbf{J}\cos(\boldsymbol{\alpha})\mathbf{F_{max}}\tilde{\mathbf{f}}_{\mathbf{P}} - \mathbf{J}_{\bar{\mathbf{m}}}\cos(\boldsymbol{\alpha})\mathbf{F_{max}}\tilde{\mathbf{f}}_{\mathbf{A}}\mathbf{a}_{\bar{\mathbf{m}}}$, eq. (6) simplifies to:

$$\boldsymbol{\tau} - \tilde{\boldsymbol{\tau}} = -\mathbf{J_m}\cos(\boldsymbol{\alpha})\mathbf{F_{max}}\tilde{\mathbf{f}}_{\mathbf{A}}\mathbf{M_m}\boldsymbol{\gamma}_{\mathbf{m}} \tag{7}$$

which is a linear equation of the form $\mathbf{y} = \mathbf{X}\boldsymbol{\beta}$. Being eq. (7) in the same form as eq. (5), the vector $\boldsymbol{\gamma_m}$ can be estimated based on measurements of $\boldsymbol{\tau}$ and $\mathbf{M_m}$ using the same process described for the MSK estimator.

C. Model-based characterization of the estimators

To investigate the accuracy of our proposed estimator compared to the standard estimation methods, we simulated virtual calibration experiments, where the quantities $\mathbf{M}_m$ and $\boldsymbol{\tau}$ are measured for a given experimental protocol, composed of N tasks (Fig. 1B, Sec. II-D). Each task is defined as an isometric contraction, applied at a given joint posture under the application of a given torque. For each contraction, the MSM

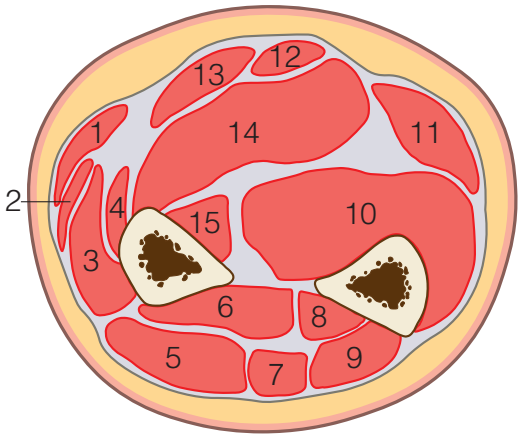

Fig. 2. Schematic of the transverse section of the forearm. In order: 1. Brachioradialis, 2. Extensor Carpi Radialis Longus, 3. Extensor Carpi Radialis Brevis, 4. Pronator Teres, 5. Extensor Digitorum Communis, 6. Abductor Pollicis Longus, 7. Extensor Digiti Minimi, 8. Extensor Pollicis Longus, 9. Extensor Carpi Ulnaris, 10. Flexor Digitorum Profundus, 11. Flexor Carpi Ulnaris, 12. Palmaris Longus, 13. Flexor Carpi Radialis, 14. Flexor Digitorum Superficialis, 15. Flexor Pollicis Longus

TABLE I
MUSCLE GROUPS IN THE MODEL

Group	Muscle Name	Abbreviation
Wrist	Extensor Carpi Radialis Brevis	ECRB
	Extensor Carpi Radialis Longus	ECRL
	Extensor Carpi Ulnaris	ECU
	Flexor Carpi Radialis	FCR
	Flexor Carpi Ulnaris	FCU
Palm	Palmaris Longus	PL
Thumb	Extensor Pollicis Brevis	EPB
	Extensor Pollicis Longus	EPL
	Abductor Pollicis Longus	APL
	Flexor Pollicis Longus	FPL
Finger	Extensor Digirotum Communis*	EDC
	Extensor Indicis Proprius	EIP
	Extensor Digiti Minimi	EDM
	Flexor Digitorum Superficialis*	FDS
	Flexor Digitorum Profundus*	FDP

* muscle composed of different segments, one per each finger: Index (I), Middle (M), Ring (R), Little (L). Since the model does not describe individual finger motion, a single muscle including all these segments is considered in this work.

produces simulated values of muscles activity for all muscles using its standard solver [26], based on the minimization of the global activation level (GAL=$\sum_i a_i^2$). For a given experimental design, the accuracy of the estimate will largely depend on the validity of the estimator assumptions and on the precision of the measurements. We have, then, introduced several sources of non-ideality in our simulations to quantify the effect of physiological variability and measurement error under different experimental conditions on the accuracy of the estimators.

1) Experimental conditions: An important factor that is expected to affect the accuracy of the estimation relates to the way the arm is constrained during the isometric contractions. In the specific case of the forearm, finger muscles have moment arm about the wrist, but they are not always accessible using sEMG (see Fig. 2 and Tab. I). As such, unmeasured activity from finger muscles could have an effect on calibration procedures that relate measured activation to wrist joint torque. Activity from finger muscles can be mediated by proper experimental design: if the fingers are unconstrained and subjects are instructed to apply wrist torque without moving their fingers, we expect that finger muscles activations will be much lower than if the fingers and palm are all constrained in a single posture (e.g. using a rigid support for the hand). In our framework, we implemented the possibility to include or neglect the contribution of finger muscles when generating virtual measurements for models that include a different total number of muscles m_{tot} (factor Ex).

2) Measurement properties: The quality of estimation crucially depends on how measurements of muscle activity are obtained, which is defined in terms of which muscles are measured (Me_1), and how much noise is included in these measurements (Me_2 and Me_3).

We considered the effect of two cascaded sources of noise: one related to the cross-talk between each muscle and those surrounding it (Me_2), and the other related to measurement error at the individual muscle level (Me_3). To define levels of factor Me_2, we assumed that the measurement of the activation for a given muscle is affected by the activity of surrounding muscles as described by the equation:

$$\mathbf{M_1} = (\epsilon^C \mathbf{C} + \mathbf{I})\mathbf{M_m} \tag{8}$$

where ϵ^C is a gain factor, $\mathbf{I}$ is the identity matrix, $\mathbf{M_m} = \mathbf{a}\boldsymbol{\gamma}_{\boldsymbol{m}}^{-1}$ is the measurement corresponding to the true value of activation $\mathbf{a}$, and $\mathbf{C}$ is a cross-correlation matrix that represents how much the measurement M_1 of one muscle is affected by the activation of all other muscles in the limb. Since no methods have been proposed to reliably estimate the crosstalk between all muscles in the limb [27], and since the amount of crosstalk highly depends on the relative position of the sEMG electrodes [28], [29] it was not possible to extract the matrix C purely from experimental data. As such we heuristically defined its elements based on proximity and relative size of the pairs of muscles (Fig. 2). To more closely resemble the experimental observations obtained for the correlation between two neighboring muscles in the forearm [29], we have considered the correlation between two proximal muscles to range between 0.3 and 0.6. For non-adjacent muscles, we accounted for inter-muscle distance comparing it to a characteristic length that, for forearm muscles, is equal to 1/8 of the forearm circumference, as shown in a computational model of propagation of electrical signal in the forearm [30]. As such, we assigned weights of zeros for muscles that were more than three characteristic lengths apart from each other and heuristically scaled the weights for muscles that were, instead, within three characteristic lengths. For proper scaling of within- and between-muscle errors, the sum of the elements for each row has unitary magnitude, with zeros in the diagonal (Tab. II).

As for the measurement error, there are different factors that concur in determining its magnitude [31] including the contact impedance [32], the electrode shape and size [33], and the location of the electrodes relative to the muscle [34].

TABLE II
MUSCLE CROSS-CORRELATION MATRIX C

	ECRB	ECRL	ECU	FCR	FCU	PL	EPL	FPL	APL	FDS	FDP	EDC	EIP	EDM
ECRB	0	0.25	0	0	0	0	0	0.1	0.15	0.1	0	0.4	0	0
ECRL	0.5	0	0	0	0	0	0	0.1	0	0	0	0.4	0	0
ECU	0	0	0	0	0	0	0.2	0	0.1	0	0.5	0	0	0.2
FCR	0.1	0.05	0	0	0	0.3	0	0	0	0.55	0	0	0	0
FCU	0	0	0	0	0	0	0	0	0	0.5	0.5	0	0	0
PL	0	0	0	0.3	0.15	0	0	0	0	0.55	0	0	0	0
EPL	0	0	0.2	0	0	0	0	0	0.35	0	0.35	0	0	0.1
FPL	0	0	0	0	0	0	0	0	0.1	0.45	0.45	0	0	0
APL	0.15	0	0	0	0.05		0.15	0.15	0	0	0	0.4	0	0.1
FDS	0.05	0.05	0	0.1	0.2	0.1	0	0.1	0	0	0.4	0	0	0
FDP	0	0	0.1	0	0.25	0	0.1	0	0.1	0.45	0	0	0	0
EDC	0.3	0	0.05	0	0	0	0.05	0	0.4	0	0	0	0	0.2
EIP	0	0	0.2	0	0	0	0	0	0.1	0	0	0.5	0	0.2
EDM	0	0	0.2	0	0	0	0.2	0	0.3	0	0	0.3	0	0

Specifically Piervirgili *et al.* showed that the level of noise is highly affected by the treatment of the skin prior to the application of the electrodes, with the noise level of the "no treatment" condition that is of the same order of magnitude of the EMG measured during common activities of daily living. As such, we considered that the muscle activity has an additive independent noise, as defined by

$$\mathbf{M_2} = \max(\mathbf{M_1} + \boldsymbol{\epsilon}^{\mathbf{M}}\bar{M}, 0) \tag{9}$$

where $\mathbf{M_1}$ is the vector obtained using eq. (8) and $\bar{M}$ is the average value of the measurements $\mathbf{M}$, simulated in the optimal control strategy, across muscles and tasks. The gain factor $\boldsymbol{\epsilon}^{\boldsymbol{M}}$ is a diagonal matrix. Since activation is a positive quantity, and since EMG is accordingly rectified, we set the lower bound of the quantity M_2 to be 0.

3) Physiological variability: Physiological variability (Ph) accounts for the intra-subject variability associated with the selection of the contraction strategy for tasks that require coordinated muscles activation [35], [36]. We modeled this variability assuming that, when solving for activation values compatible with the target joint torque, the virtual subject selects a suboptimal solution (different from the optimal one), whose *suboptimality level* is defined in term of percentage of additional GAL used to complete the isometric task:

$$\sum a_{sub}^2 = \sum a_{opt}^2 + \epsilon^A \overline{\text{GAL}}_{opt} \tag{10}$$

where $\overline{\text{GAL}}_{opt}$ is the average GAL_{opt} across the different tasks, and ϵ^A a gain factor.

D. Sensitivity analysis

We conducted virtual calibration experiments (Fig. 1B) where muscle activity was simulated under different levels of the previously described factors to assess the robustness of the two estimators to changes in experimental conditions, measurement properties, and physiological variability.

Factor levels were defined as follows (Fig. 3). We considered two levels of factor Ex, i.e. fingers unconstrained/constrained. In the unconstrained mode, we assumed negligible the activation of finger muscles and their passive forces. In the constrained mode, instead, the full model (including forearm, hand, fingers muscles) was considered. Also for the factor Me_1 we considered two different levels: the first level corresponding to the case where measurements are available only from the five main wrist muscles (MeasWrist), i.e. ECRL, ECRB, ECU, FCR, FCU, and the second level corresponding to the case where measurements are available from all muscles included in the model (MeasAll).

Values of factors representing a continuous source of noise/variability (i.e. Me_2, Me_3, Ph) were, then, selected from uniform distributions, $\epsilon^C \in [0, \epsilon^C_{max}]$, $\epsilon^M_{i,i} \in [-\epsilon^M_{max}, \epsilon^M_{max}]$, $\epsilon^A \in [0, \epsilon^A_{max}]$, with a different value selected for each contraction. For all three factors, five levels of $\epsilon^{\bullet}_{max}$ were considered ($\epsilon^{\bullet}_{max} = [0\ 0.1\ 0.25\ 0.5\ 1]$).

This analysis resulted in a full factorial experimental design (5x5x5x2x2) composed of 500 combinations (Fig. 3). For each combination, we simulated $N = 25$ virtual experiments, each composed of 25 isometric contractions, applied in five different wrist postures ($[\theta_{FE}, \theta_{RUD}] \in \{[-30, 0], [-15, 0], [0, 0], [15, 0], [30, 0]\}$), when constant torque was applied along each of the four cardinal directions (pure wrist FE and wrist RUD torque in both directions), with unitary magnitude, followed by a rest condition (zero joint torque). For each contraction, we simulated measurements of muscle activity by assuming $\boldsymbol{\gamma}_m = 10$ for all measured muscles.

For each experiment, we then estimated $\hat{\gamma}_m$ using both MSK and NMSK, and quantified the accuracy of each estimator as the bias $\bar{b}$, defined as the percent error in estimating γ_m for the five main wrist muscles, averaged across muscles.

1) Statistical model fit: To establish the relationship between the factors and the outcome metric $\bar{b}$, we fit a General Linear Model (GLM) to the simulated data. Ph, Me_2, and Me_3 were modeled as ordinal variables characterized by the mean value of $|\epsilon^{\bullet}|$ across the 25 contractions. Ex and Me_1 are instead modeled as categorical variables. Specifically, Ex assumed the value of 0 if the fingers joint were constrained and 1 if they were unconstrained, while Me_1 assumed value of 0 if the measurements were available from all muscles and 1 if they were available only from the five main wrist muscles. Moreover, a third categorical variable E was used to include the factor 'estimator' in the GLM; we assigned the value of 0 to MSK and the value of 1 to NMSK.

To quantify the relationship between estimation bias ($\bar{b}$),

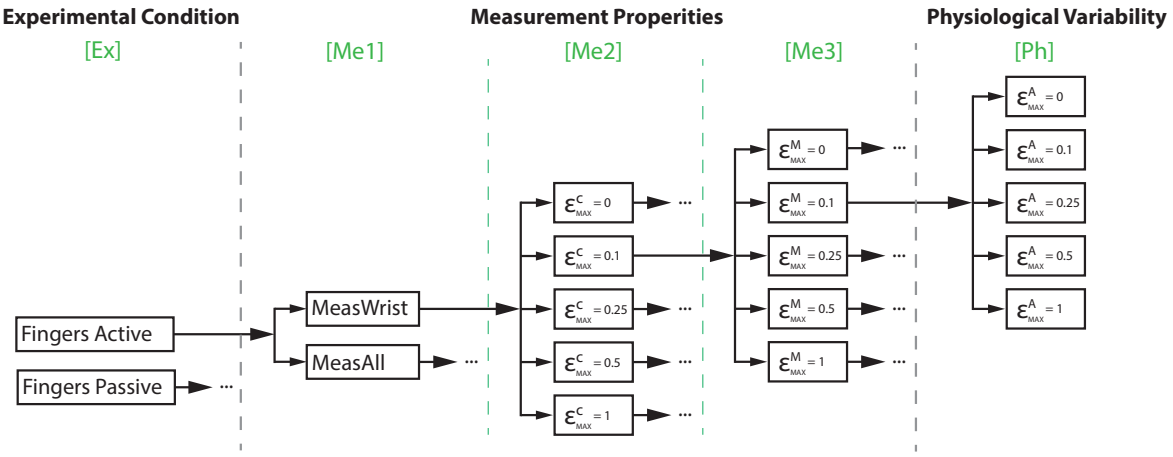

Fig. 3. Diagram of the factorial experimental design used for the sensitivity analysis. The columns, delineated by the dashed lines, represent the different factors included in the analysis. Within each column, the different levels of the factor are displayed. The branching of the design is shown for a representative combination, denoted by solid arrows crossing the dashed lines. The '...' indicates that all downstream branches are replicated.

measurement error (Me_2, Me_3), and physiological variability (Ph), under all possible experimental and measurement conditions encoded by categorical variables (E, Ex, Me_1), we created a GLM that included all interactions between the three categorical variables, as well as the interactions between all combinations of categorical variables and Me_2, Me_3, Ph, separately. This resulted in a model with 32 factors, which included 3 four-way interaction terms, 10 three-way interaction terms, 12 two-way interaction terms, in addition to the linear contribution of the 6 factors and the intercept. Statistically significant association between the metric $\bar{b}$ and each term in the GLM was considered for a type-I error rate smaller than 0.05.

To allow for visualization and interpretation of effects, for each significant term, we defined residual bias as the difference between the simulated bias $\bar{b}$, and the bias b_{other} calculated as the bias explained by all terms that do not include any factor in the significant term (e.g. for the term E·Me_1, we would include in b_{other} the components estimated by the model that do not include factors E and Me_1). This operation was conducted assuming that all other factors in the model were at their average level. This allowed to obtain distributions of residual bias for each combination of factors included in the significant term (2 for a main effect, 4 for a two-way interaction, etc.), which could be visually checked for model fit by comparing the distribution of $\bar{b} - b_{other}$ with the corresponding model values, and to identify which combination of factors contributes to the significance of the term.

TABLE III
RESULTS OF THE GENERAL LINEAL MODEL FITTING

	Estimate	SE	tStats	p
Intercept	0.0002	0.0052	0.0452	0.9639
E	0	0.0073	0	1
Ex	0.0033	0.0077	0.4351	0.6635
Me_1	0.0297	0.0073	4.0318	<0.001
Ph	0.0014	0.0142	0.1026	0.9183
Me_2	0.0002	0.0141	0.0155	0.9876
Me_3	0.1052	0.0142	7.3982	<0.001
E ·Me_1	-0.0236	0.0104	-2.2718	0.0233
E · Ex	0	0.0109	0	1
E · Ph	0	0.0209	0.0200	1
E · Me_2	0	0.0200	0	1
E · Me_3	0	0.0201	0	1
Ex · Me_1	0.2772	0.0106	25.9370	<0.001
Ex · Ph	0.0680	0.0209	3.2462	0.0012
Ex · Me_2	0.2723	0.0210	12.9150	<0.001
Ex · Me_3	0.7847	0.0229	34.1810	<0.001
Me_1 · Ph	0.0445	0.0200	2.2186	0.0267
Me_1 · Me_2	-0.0014	0.0200	-0.0696	0.9444
Me_1 · Me_3	-0.0656	0.0201	-3.2638	0.0011
E · Ex · Me_1	-0.2785	0.0151	-18.433	<0.001
E · Ex · Ph	0	0.0296	0	1
E · Ex · Me_2	0	0.0298	0	1
E · Ex · Me_3	0	0.0324	0	1
E ·Me_1 · Ph	0.0181	0.0284	0.6383	0.5234
E ·Me_1 · Me_2	0.0002	0.0282	0.0061	0.9950
E ·Me_1 · Me_3	0.0158	0.0284	0.5581	0.5769
Ex · Me_1 · Ph	0.0053	0.0290	0.1833	0.8545
Ex · Me_1 · Me_2	-0.0644	0.0292	-2.2044	0.0277
Ex · Me_1 · Me_3	-0.8526	0.0305	-27.9280	<0.001
E · Ex · Me_1 · Ph	-0.0399	0.0411	-0.9692	0.8545
E · Ex · Me_1 · Me_2	0.0219	0.0412	0.5306	0.5957
E · Ex · Me_1 · Me_3	0.3096	0.0431	7.1730	<0.001

III. RESULTS

The results of the sensitivity analysis are graphically summarized in Fig. 4, where each dot represents the average value of the metric $\bar{b}$ obtained for each set of factors in the 25 different repetitions. The GLM fit the simulated data with an $R^2 = 0.96$. The coefficients estimated for all model terms, along with the standard error (SE), the test statistics (tStats) and the level of significance (two-sided tests) are reported in Tab. III.

Model fit identified a significant main effect of only two of the six factors, Me_1 and Me_3 ($p < 0.001$ for both) (Fig. 5). Specifically, the bias explained by only factor Me_1, when all other factors were in their average conditions, was significantly smaller in the MeasAll condition than in the MeasWrist condition (mean ± 95% confidence interval - 0.11±0.01 MeasAll, vs. 0.14±0.01 MeasWrist). For Me_3, each unit increase in measurement error ϵ_M resulted in an increase in residual bias of 0.29 when all other factors were in their average conditions.

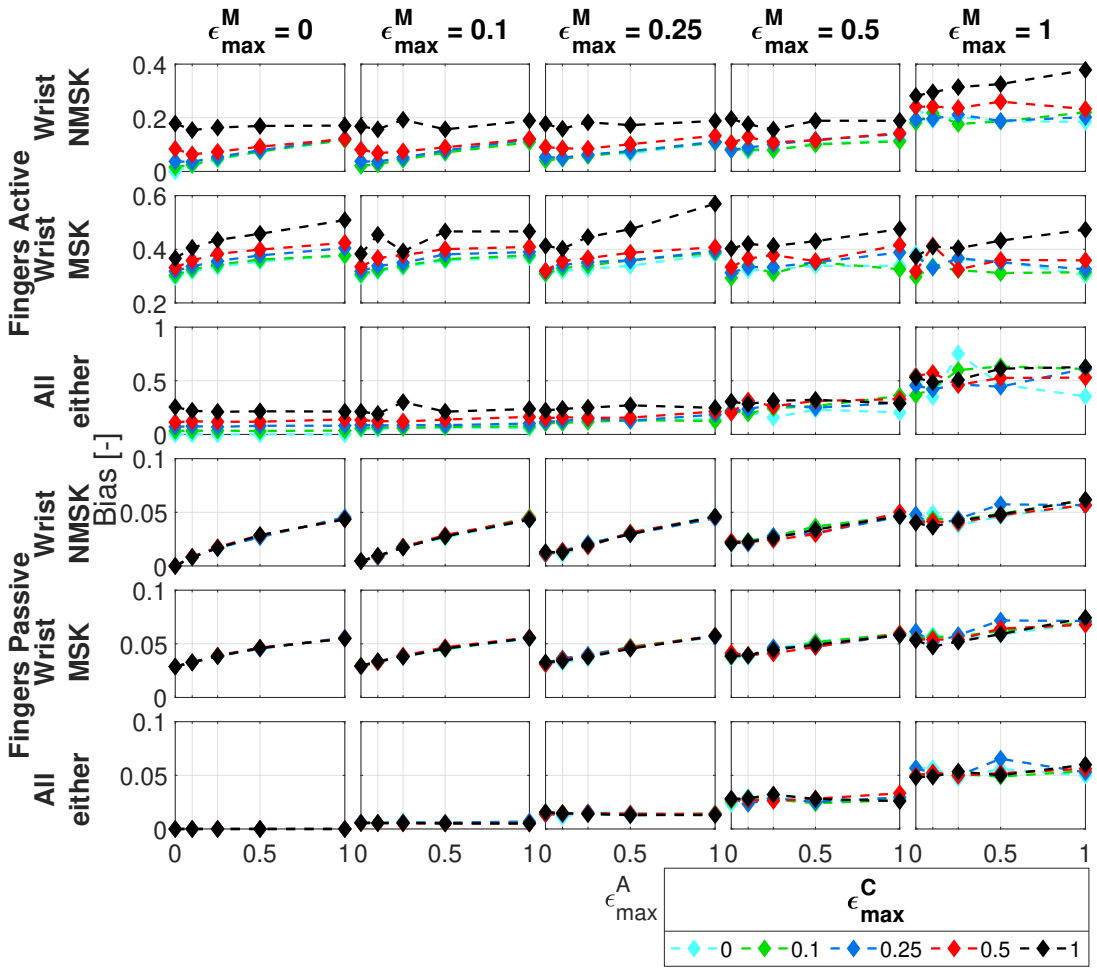

Fig. 4. Values of metric $\bar{b}$ obtained for all levels of all factors. The top three rows include results obtained in presence of finger muscles (Ex=1), while the bottom three rows report the results obtained in the absence of finger muscles (Ex=0). The first two rows of each of subgroup report bias obtained when measurements are available from only wrist muscles (Me_1 = 1), while the third row reports results obtained when measurements are available from all muscles (Me_1 = 0). Rows one and four include estimation results obtained with the NMSK estimator (E=1), while rows two and five are obtained with the MSK estimator (E=0). Rows three and six are obtained with either estimator since no difference is expected when measurements are available from all muscles. Columns encode levels of factor Me_3 (measurement error), colors encode levels of factor Me_2 (cross-talk), while the x-axis of each plot encodes levels of factor Ph (physiological variability).

Seven two-way interaction terms had a statistically significant effect, i.e. E·Me_1 (p = 0.0233), Ex·Me_1 (p <0.001), Ex·Ph (p = 0.0012), Ex·Me_2 (p <0.001), Ex·Me_3 (p <0.001), Me_1·Ph (p = 0.0267), Me_1·Me_3 (p = 0.0011). Further analysis of the effects of the two-way interactions is excluded from this section for the sake of space. All significant effects are broken down in the interaction plots shown in Fig. 6, when all other factors are in their average condition.

Model fit identified as statistically significant three three-way interaction terms, i.e. E·Ex·Me_1 (p <0.001), Ex·Me_1·Me_2 (p = 0.0277), Ex·Me_1·Me_3 (p <0.001) (Fig. 7), and one four-way interaction term, E·Ex·Me_1·Me_3 (p <0.001) (Fig. 8). For the interaction between E, Ex, and Me_1 (Fig. 7, top row), the NMSK estimator introduced a statistically significant decrease in estimation bias over the MSK estimator in the MeasWrist condition (0.05±0.01 MSK vs. 0.03±0.01 NMSK, fingers passive; and 0.36±0.02 MSK vs. 0.12±0.02 NMSK, fingers active), but the effect of the estimator was greater when fingers were active than when fingers were passive (change in bias: 0.02 ± 0.01 fingers passive, vs. 0.24±0.03 fingers active). As expected, no difference between the two estimators was observed in the MeasAll condition; in that condition, bias was greater when fingers were active than when they were passive (0.2±0.02, fingers active vs. 0.02±0.02, fingers passive).

For the interaction between Me_1, Ex, and Me_2 (Fig. 7, middle row), cross-talk introduced no significant effect on bias when fingers were passive (slope: 0± 0.1 in both cases), but bias significantly increased in the MeasWrist condition (bias: 0.02±0.01 MeasWrist vs. 0.03±0.01 MeasAll). Instead, when fingers were active, a significant effect of cross-talk was measured in both the MeasAll and the MeasWrist condition (slope: 0.22±0.08 for MeasWrist vs 0.27±0.09 for MeasAll). However, no significant difference between the two slopes was measured. In general, regardless of the value of cross-talk, in the finger active condition, bias in the MeasWrist condition was always larger than bias in the MeasAll condition (bias: 0.19±0.01 for MeasAll vs. 0.24±0.01 MeasWrist), as seen in Fig. 6A, second row and Fig. 7.

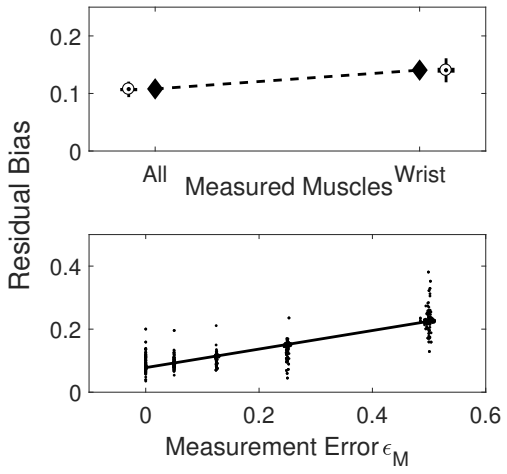

Fig. 5. Graphical representation of the linear contribution of the two statistically significant predictors. In the top row the diamonds represents the model estimates, with the simulated data reported in the error bar. In the bottom row the line represents the model estimate while the points are the simulated data. All plots are obtained in the average condition of noise for the unreported variables. Note that ϵ_M is the average of the $\epsilon_{i,j}^M$ values randomly selected from the distribution $[-\epsilon_{max}^M, \epsilon_{max}^M]$ for the different muscles and tasks.

For the interaction between Me_1, Ex, and Me_3 (Fig. 7, bottom row), measurement error was significantly associated with bias in all cases when fingers were active (0.96±0.11 MeasAll, and 0.15±0.09 MeasWrist), while a significant association was measured only in the MeasAll condition when fingers were passive (slope: 0.1±0.08 MeasAll, 0.5±0.09 MeasWrist). The association between measurement error and bias was significantly modulated by factor Me_1: in the MeasAll condition, the slope was greater than in the MeastWrist condition ($p < 0.05$).

Lastly, for the three four-way interactions (Fig. 8), estimation bias obtained with the NMSK estimator was not significantly different from the one obtained with the MSK estimator in the absence of finger muscles, and in the MeasAll condition when fingers are present. This was expected because of the presence of a significant effect of E only in the fingers active, MeasWrist condition. In this condition, further breakdown of the three-way interaction by variability/noise source showed that the three-way interaction is significant because of a different effect of Me_3, whereby the slope between measurement error and bias is greater in the NMSK estimator than in the MSK estimator, in the finger active, MeasWrist condition (slope: 0.32±0.13 NMSK vs. -0.03±0.13 MSK). For physiological variability, instead, the slope between these variables and bias did not change significantly between estimators in the finger active, MeasWrist condition (slope: 0.10±0.12 NMSK vs. 0.12±0.12 MSK). Most notably, the effect of Ph on bias was not significant for neither estimator at the selected significance level. For cross-talk, instead, a signifiant association with bias was observed for both estimators (slope: 0.25±0.12 NMSK vs. 0.22±0.1 MSK), while no significant difference in slope between estimators was detected at the selected significance level.

IV. Discussion

In this study, we proposed a novel neuromusculoskeletal (NMSK) estimator that combines a standard forward dynamics estimation approach with a neural model that determines the activation of unmeasured muscles, using an optimization-based redundancy solver. We hypothesized that this novel estimator would be able to estimate individual muscle force with greater accuracy compared to a standard musculoskeletal (MSK) estimator, when measurements of muscle activity are not available for all muscles.

To test our hypothesis, we ran a sensitivity analysis to quantify the effect of a set of experimental, physiological, and measurement conditions on the accuracy of muscle force estimation, both for our NMSK estimator and for the MSK estimator. To this goal, we developed a computational framework capable of simulating virtual measurements of muscle activity under a variety of experimental conditions, physiological variability and measurement error. Then, by fitting the estimation error to a general linear model, we established the association between different experimental factors and the estimation bias that characterize each estimator.

Overall, our statistical analysis demonstrated that the MSK estimator, used in standard procedures to study control of the wrist degrees of freedom [11], [29], produces biased estimates of individual muscle force in presence of activity of finger muscles. However, when measurements are available from only the five main wrist muscles, the estimation bias obtained with the NMSK estimator is significantly smaller than the one obtained with the MSK estimator. Our statistical analysis further demonstrated that the effect of cross-talk on bias is greater when fingers are active compared to when fingers are passive, for either estimator. Moreover, measurement error has a greater effect on bias when fingers are active compared to when fingers are passive, but the effect is greater when measurements are obtained from all muscles. Finally, while our NMSK estimator is heavily model-based, the lack of a significantly different association between physiological variability and bias (in all conditions) provides an indication of the robustness of the NMSK estimator with respect of violations of its assumptions in the identification of the optimal solution to muscle redundancy. A more detailed discussion of our main findings is reported below.

A. Effect of estimator

Our analysis did not detect a main effect of factor estimator (E). In fact, estimator type has a significant effect on bias only under one condition: when measurements are taken only from wrist muscles (MeasWrist) (Fig 7, see also Fig. SM1). This was expected, because when measurements are available from all muscles (MeasAll), the MSK and NMSK estimators are identical. In the MeasWrist condition, the NMSK estimator produced a statistically significant decrease ($p < 0.05$) in the amount of estimation error in 122 of the 125 simulation conditions when the finger muscles were considered active, and in all 125 conditions, when the finger were passive (Fig. SM1). Overall, in average noise condition the NMSK estimator reduces estimation bias over the MSK estimator (change in

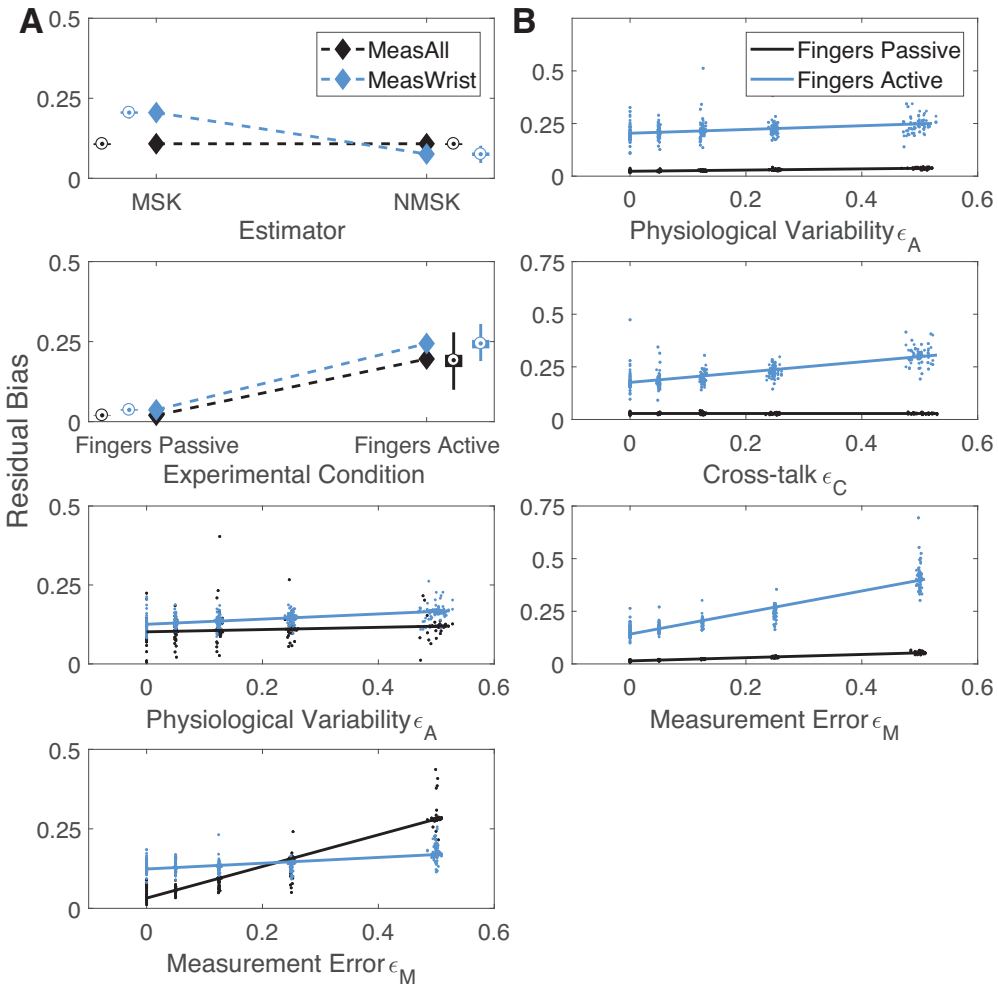

Fig. 6. Graphical representation of the statistically significant two-way interaction terms. In the top two rows the diamonds and the lines represents the model estimates, while the simulated data reported in term of error bars or scattered dots. All plots are obtained in the average condition of noise for the unreported variables. Columns A and B report the statistically significant two-interaction terms that involve the factors Me_1 and Ex, respectively.

bias: 2±1% for finger passive, 24±3%for fingers active in the average noise conditions). The greater effect seen in the active condition is justified by the fact that in the fingers active condition, the set of unmeasured muscles is composed by n =10 muscles, while in the passive condition there is only one unmeasured muscle (i.e. PL).

A second effect of factor estimator was observed in the difference in slope of the relationship between measurement error and bias measured in the finger active, MeasWrist condition for the two estimators (slope: 32±13% NMSK vs -3±13% MSK). While this result indicates that the NMSK estimator is more sensitive to measurement error than the MSK estimator, the bias obtained using the NMSK estimator is smaller than the one obtained using the MSK estimator for all values of measurement error in the considered range.

Notably, no interaction between estimator and physiological variability was detected. As such, physiological variability is not significantly associated with bias for either estimator (slope: 10%±12%for NMSK vs. MSK 12%±12%). While this effect was expected for the MSK estimator, this was unexpected for the NMSK since this estimator is based on a neural model of muscle activation, and physiological variability effectively quantifies the distance between the assumed model and experimental conditions. The lack of a significant difference between the slopes associated with the two estimators indicates that the NMSK estimator does not provide a worse estimation compared to the standard MSK estimator even under strong violations of the validity of the assumed neural model. This observation provides an indication of the robustness of the NMSK estimator to changes in muscle co-contraction strategy. This observation is justified by the fact that also the assumption under the MSK estimator is an implicit neural model, i.e. that all muscles that are not measurable are inactive. This is a possibly inefficient solution to the muscle redundancy problem. Our analysis demonstrates that a model-based estimator that is based on a largely inaccurate neural model outperforms the standard MSK estimator based on such an implicit neural model.

B. Effect of number of measured muscles

Our analysis detected a main effect of the number of measured muscles (Me_1). Unsurprisingly, estimation performed

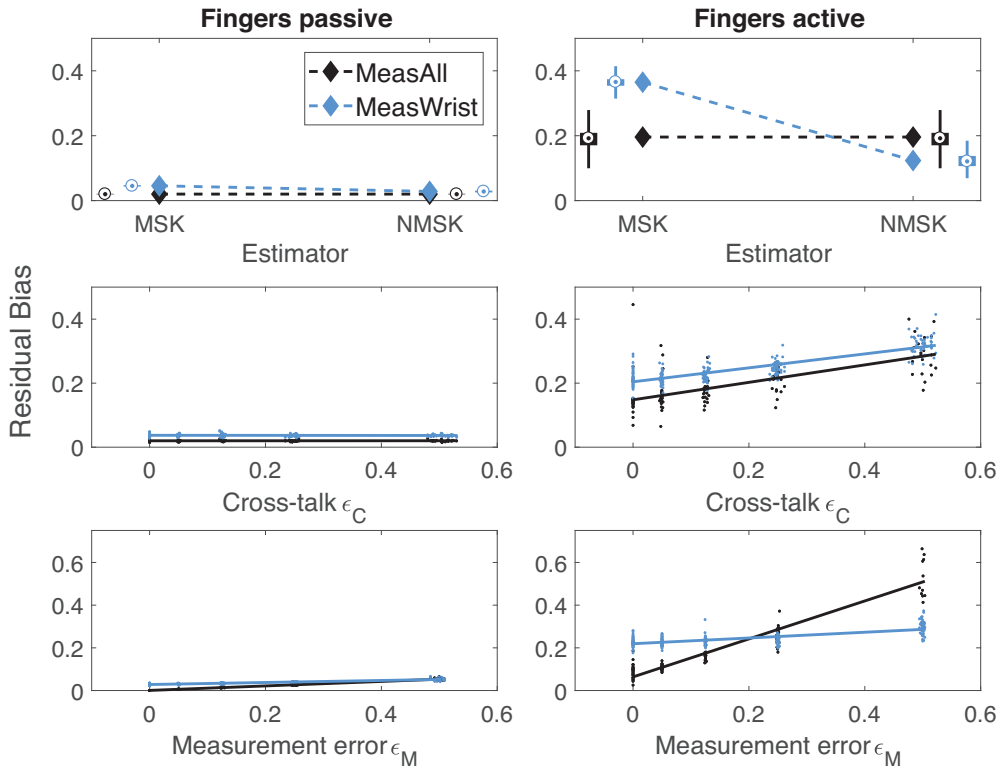

Fig. 7. Graphical representation of the statistically significant three-way interaction terms. In the top row the diamonds represents the model estimates, with the simulated data reported in the error bar. In the central and bottom rows the lines represents the model estimates while the points are the simulated data. All plots are obtained in the average condition of noise for Ph, Me_2 and Me_3

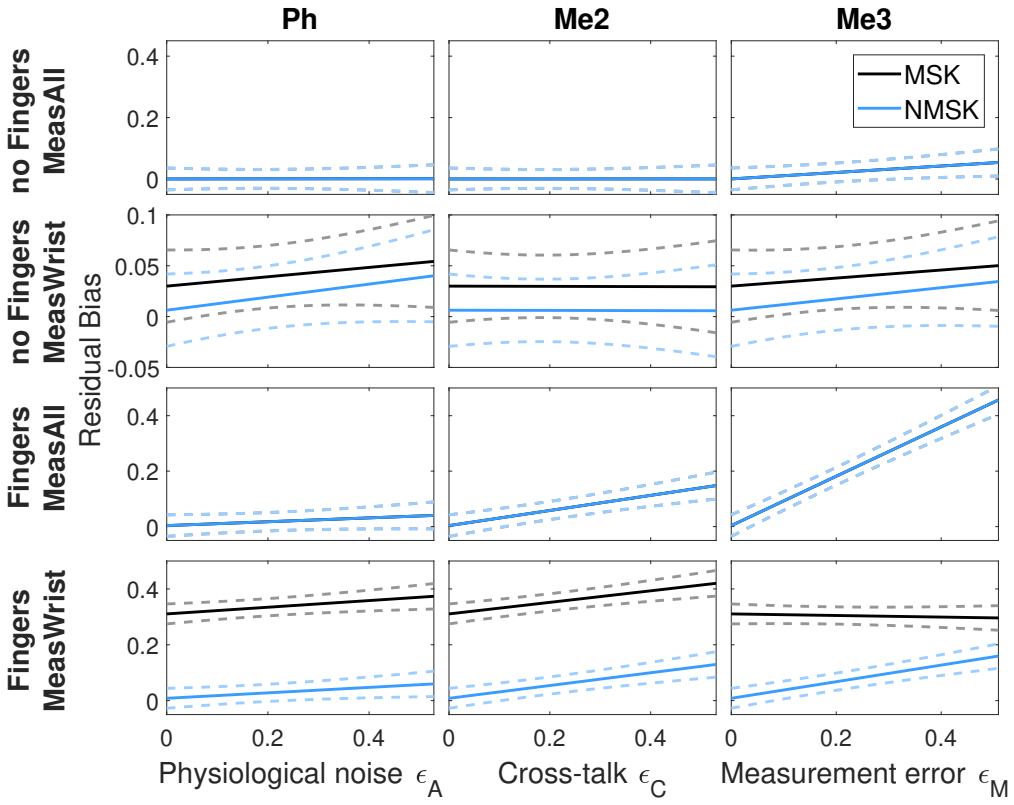

Fig. 8. Graphical representation of the four-way interaction terms between the three categorical variables (E, Ex, Me_1) and Ph (first column), Me_2 (second column), and Me_3 (third column). In each plot the sold line represents the model estimate and the dashed lines the 95% confidence intervals.

using the complete set of muscles yielded a smaller bias compared to the one performed based on a restricted set of muscles (bias: 11%±1 MeasAll vs. 14%±1 for MeasWrist).

Factor Me_1 showed a significant interaction with cross-talk and experimental condition (Fig. 7, middle row). Specifically, the interaction showed that bias is associated with cross-talk only if the finger muscles are in the active condition. While this result certainly depends on the choice of the cross-correlation matrix C, it confirms previous analyses [28], [29] that suggested how the presence of finger muscles could introduce significant cross-talk in sEMG calibration studies from the forearm.

Factor Me_1 showed a significant interaction with measurement error and experimental condition (Fig. 7, bottom row). Specifically, the interaction showed that bias is only associated with measurement error if the finger muscles are active. Interestingly, in this condition model fit lines intersect, indicating that, in presence of high levels of measurement error, the estimation error is lower when measurements are available from a reduced set of muscles compared to when measurements are available from the complete set of muscles. We believe that this effect is attributable to the fact that in presence of extremely high measurement error, the values of activation estimated by the neural model become more accurate than the ones obtained with the measurements. As a consequence, the MeasAll condition is characterized by a greater variability compared to the MeasWrist one, leading to a greater estimation error.

C. Limitations

Some limitations of this study should be considered regarding the selection of the parameters in the sensitivity analysis and applicability of our novel neuromusculoskeletal estimator to real experimental protocol. Ranges for the parameters that define the non-idealities included in the sensitivity analysis–i.e. measurement error, cross-talk, and physiological variability–have been identified via analysis of the literature. Unfortunately, the exact value of each of these parameters could not be retrieved, since that would require the use of gold-standard measurement methodologies to obtain the true value of muscle force or activation for all muscles. However, using controlled experimental conditions previous studies have quantified the effect of the different noise sources in a way that they are directly relevant for our analysis [28]–[36]. While it would not be possible to quantify the accuracy of muscle force estimators using purely experimental data, this simulation study serves as a preliminary validation tool to investigate the robustness of the estimators to variation of the noise levels in the experimental data.

As for the applicability of our novel estimator to quantify individual muscle force during real experimental data acquisition, additional work needs to be done to implement subject-specific scaling of the MSM to subject's anthropometry. [37], [38]. This procedure is required for all model-based estimators [13] and it is necessary due to te fact that the musculoskeletal model, used to determine the parameters of the MT units, represents the anthropometry of an average healthy individual.

Finally, while at the current state the proposed estimator can only be employed to estimate muscle forces during isometric tasks, this estimator can be extended to work also during dynamic tasks with some modifications. Specifically, an inverse dynamic algorithm should be included in the 'redundancy solver' block of the estimator (Fig. 1A) to determine the optimal time-varying muscle activation patterns that, for the measured torque and position, minimize GAL while maintaining continuity and smoothness constraints [26]. Moreover, eq. (1) needs to be modified to model force-velocity dependence that characterize musculotendon dynamics [13], [25]. The presented calibration protocol can then be extended to dynamic conditions to estimate the muscle-specific parameter γ.

V. Conclusion

Our analysis shows that estimating the forces applied by the forearm muscles during isometric tasks that involve the wrist joint can be challenging. In fact, by relying only on the EMG measurements obtained from the five main wrist muscles (i.e. MSK estimator), highly biased estimates of individual muscle force are obtained when fingers are active (average bias of 36±2%). Even though leaving the fingers unconstrained decreases estimation bias, this procedure is not always practically possible and it still requires to train subjects to not activate finger muscles during data collection. Instead, the integration in the estimator of a neural model of the optimal muscle co-contraction strategy (i.e. NMSK estimator) reduces the estimation bias by about 25% of the true value. Moreover, even when the validity of the neural model used for the NMSK estimator is compromised, the NMSK estimator still outperforms the MSK estimator.

References

[1] W. Herzog, "Skeletal muscle mechanics: Questions, problems and possible solutions Daniel P Ferris," *Journal of NeuroEngineering and Rehabilitation*, vol. 14, no. 1, pp. 1–17, 2017.

[2] A. Erdemir, S. McLean, W. Herzog, and A. J. van den Bogert, "Model-based estimation of muscle forces exerted during movements," *Clinical Biomechanics*, vol. 22, no. 2, pp. 131–154, 2007.

[3] Y. C. Lin, T. W. Dorn, A. G. Schache, and M. G. Pandy, "Comparison of different methods for estimating muscle forces in human movement," *Proceedings of the Institution of Mechanical Engineers, Part H: Journal of Engineering in Medicine*, vol. 226, no. 2, pp. 103–112, 2012.

[4] F. C. Anderson and M. G. Pandy, "Static and dynamic optimization solutions for gait are practically equivalent," *Journal of Biomechanics*, vol. 34, no. 2, pp. 153–161, 2001.

[5] D. G. Thelen, F. C. Anderson, and S. L. Delp, "Generating dynamic simulations of movement using computed muscle control," *Journal of Biomechanics*, vol. 36, no. 3, pp. 321–328, 2003.

[6] D. Tsirakos, V. Baltzopoulos, and R. Bartlett, "Inverse optimization: functional and physiological considerations related to the force-sharing problem." *Critical reviews in biomedical engineering*, vol. 25, no. 4-5, pp. 371–407, 1997.

[7] A. J. Van Den Bogert, T. Geijtenbeek, O. Even-Zohar, F. Steenbrink, and E. C. Hardin, "A real-time system for biomechanical analysis of human movement and muscle function," *Medical and Biological Engineering and Computing*, vol. 51, no. 10, pp. 1069–1077, 2013.

[8] D. A. Winter, *Biomechanics and Motor Control of Human Movement*. New York, NY: Sons, John Wiley and, 2005.

[9] J. J. Collins, "The redundant nature of locomotor optimization laws," *Journal of Biomechanics*, vol. 28, no. 3, pp. 251–267, 1995.

[10] U. Glitsch and W. Baumann, "The three-dimensional determination of internal loads in the lower extremity," *Journal of Biomechanics*, vol. 30, no. 11-12, pp. 1123–1131, 1997.

[11] T. S. Buchanan, M. J. Moniz, J. P. A. Dewald, and W. Z. Rymer, "Estimation of muscle forces about the wrist joint during isometric tasks using an EMG coefficient method," *Journal of Biomechanics*, vol. 26, no. 4-5, pp. 547–560, 1993.

[12] T. S. Buchanan, D. G. Lloyd, K. Manal, and T. F. Besier, "Neuromusculoskeletal modeling: estimation of forces and joint moments and movements from mrasuerments of nueral command," *Journal of applied biomechanics*, vol. 20, no. 4, pp. 367–395, 2006.

[13] M. Sartori, M. Reggiani, D. Farina, and D. G. Lloyd, "EMG-Driven Forward-Dynamic Estimation of Muscle Force and Joint Moment about Multiple Degrees of Freedom in the Human Lower Extremity," *PLoS ONE*, vol. 7, no. 12, 2012.

[14] C. R. Winby, D. G. Lloyd, T. F. Besier, and T. B. Kirk, "Muscle and external load contribution to knee joint contact loads during normal gait," *Journal of Biomechanics*, vol. 42, no. 14, pp. 2294–2300, 2009.

[15] D. G. Lloyd and T. F. Besier, "An EMG-driven musculoskeletal model to estimate muscle forces and knee joint moments in vivo," *Journal of Biomechanics*, vol. 36, no. 6, pp. 765–776, 2003.

[16] M. Asefi, S. Moghimi, H. Kalani, and A. Moghimi, "Dynamic modeling of SEMG-force relation in the presence of muscle fatigue during isometric contractions," *Biomedical Signal Processing and Control*, vol. 28, pp. 41–49, 2016.

[17] J. P. Walter, A. L. Kinney, S. A. Banks, D. D. D'Lima, T. F. Besier, D. G. Lloyd, and B. J. Fregly, "Muscle Synergies May Improve Optimization Prediction of Knee Contact Forces During Walking," *Journal of Biomechanical Engineering*, vol. 136, no. 2, p. 021031, 2014.

[18] K. Manal, K. Gravare-Silbernagel, and T. S. Buchanan, "A real-time EMG-driven musculoskeletal model of the ankle," *Multibody System Dynamics*, vol. 28, no. 1-2, pp. 169–180, 2012.

[19] K. Bouillard, A. Nordez, and F. Hug, "Estimation of individual muscle force using elastography," *PLoS ONE*, vol. 6, no. 12, 2011.

[20] F. Hug, K. Tucker, J. L. Gennisson, M. Tanter, and A. Nordez, "Elastography for Muscle Biomechanics: Toward the Estimation of Individual Muscle Force," *Exercise and Sport Sciences Reviews*, vol. 43, no. 3, pp. 125–133, 2015.

[21] T. K. Koo, J. Y. Guo, J. H. Cohen, and K. J. Parker, "Relationship between shear elastic modulus and passive muscle force: An ex-vivo study," *Journal of Biomechanics*, vol. 46, no. 12, pp. 2053–2059, 2013.

[22] K. R. Saul, X. Hu, C. M. Goehler, M. E. Vidt, M. Daly, A. Velisar, and W. M. Murray, "Benchmarking of dynamic simulation predictions in two software platforms using an upper limb musculoskeletal model." *Computer methods in biomechanics and biomedical engineering*, vol. 5842, no. May 2016, pp. 1–14, 2014.

[23] A. Zonnino and F. Sergi, "Model-Based Estimation of Individual Muscle Force Given an Incomplete Set of Muscle Activity Measurements," in *Converging Clinical and Engineering Research on Neurorehabilitation III*, L. Masia, S. Micera, M. Akay, and J. L. Pons, Eds., vol. 15, no. 16. Cham: Springer International Publishing, 2019, pp. 800–804.

[24] A. V. Hill, "The heat of shortening and the dynamic constants of muscle," *Proceedings of the Royal Society of London B: Biological Sciences*, vol. 126, no. 843, pp. 136–195, 1938.

[25] M. Millard, T. Uchida, A. Seth, and S. L. Delp, "Flexing computational muscle: modeling and simulation of musculotendon dynamics," *J Biomech Eng*, vol. 135, no. 2, p. 21005, 2013.

[26] A. Seth, M. Sherman, J. A. Reinbolt, and S. L. Delp, "OpenSim: A musculoskeletal modeling and simulation framework for in silico investigations and exchange," *Procedia IUTAM*, vol. 2, pp. 212–232, 2011.

[27] D. Farina, R. Merletti, B. Indino, and T. Graven-Nielsen, "Surface EMG crosstalk evaluated from experimental recordings and simulated signals," *Methods of Information in Medicine*, vol. 43, no. 1, pp. 30–35, 2004.

[28] Y. K. Kong, M. S. Hallbeck, and M. C. Jung, "Crosstalk effect on surface electromyogram of the forearm flexors during a static grip task," *Journal of Electromyography and Kinesiology*, vol. 20, no. 6, pp. 1223–1229, 2010.

[29] J. P. Mogk and P. J. Keir, "Crosstalk in surface electromyography of the proximal forearm during gripping tasks," *Journal of Electromyography and Kinesiology*, vol. 13, no. 1, pp. 63–71, 2003.

[30] M. M. Lowery, N. S. Stoykov, J. P. A. Dewald, and T. A. Kuiken, "Volume Conduction in an Anatomically Based Surface EMG Model," *IEEE Transactions on Biomedical Engineering*, vol. 51, no. 12, pp. 2138–2147, 2004.

[31] D. Farina, R. Merletti, and R. M. Enoka, "The extraction of neural strategies from the surface EMG," *Journal of Applied Physiology*, vol. 96, pp. 1486–1495, 2004.

[32] G. Piervirgili, F. Petracca, and R. Merletti, "A new method to assess skin treatments for lowering the impedance and noise of individual gelled Ag AgCl electrodes," *Physiological Measurement*, vol. 35, pp. 2101–2118, 2014.

[33] R. Merletti, A. Botter, and U. Barone, "Detection and Conditioning of Surface EMG Signals," in *Surface Electromyography: Physiology, Engineering, and Applications*, ser. Wiley Online Books, 2016.

[34] I. Campanini, A. Merlo, P. Degola, R. Merletti, G. Vezzosi, and D. Farina, "Effect of electrode location on EMG signal envelope in leg muscles during gait," *Journal of Electromyography and Kinesiology*, vol. 17, pp. 515–526, 2007.

[35] B. Larsson, S. Karlsson, M. Eriksson, and B. Gerdle, "Test-retest reliability of EMG and peak torque during repetitive maximum concentric knee extensions," *Journal of Electromyography and Kinesiology*, vol. 13, no. 3, pp. 281–287, 2003.

[36] J. Kollmitzer, G. R. Ebenbichler, and A. Kopf, "Reliability of electromyographic measurements using surface electrodes," *Clinical Neurophysiology*, vol. 110, pp. 725–734, 1999.

[37] L. Modenese, E. Ceseracciu, M. Reggiani, and D. G. Lloyd, "Estimation of musculotendon parameters for scaled and subject specific musculoskeletal models using an optimization technique," *Journal of Biomechanics*, vol. 49, no. 2, pp. 141–148, 2016.

[38] C. R. Winby, D. G. Lloyd, and T. B. Kirk, "Evaluation of different analytical methods for subject-specific scaling of musculotendon parameters," *Journal of Biomechanics*, vol. 41, no. 8, pp. 1682–1688, 2008.

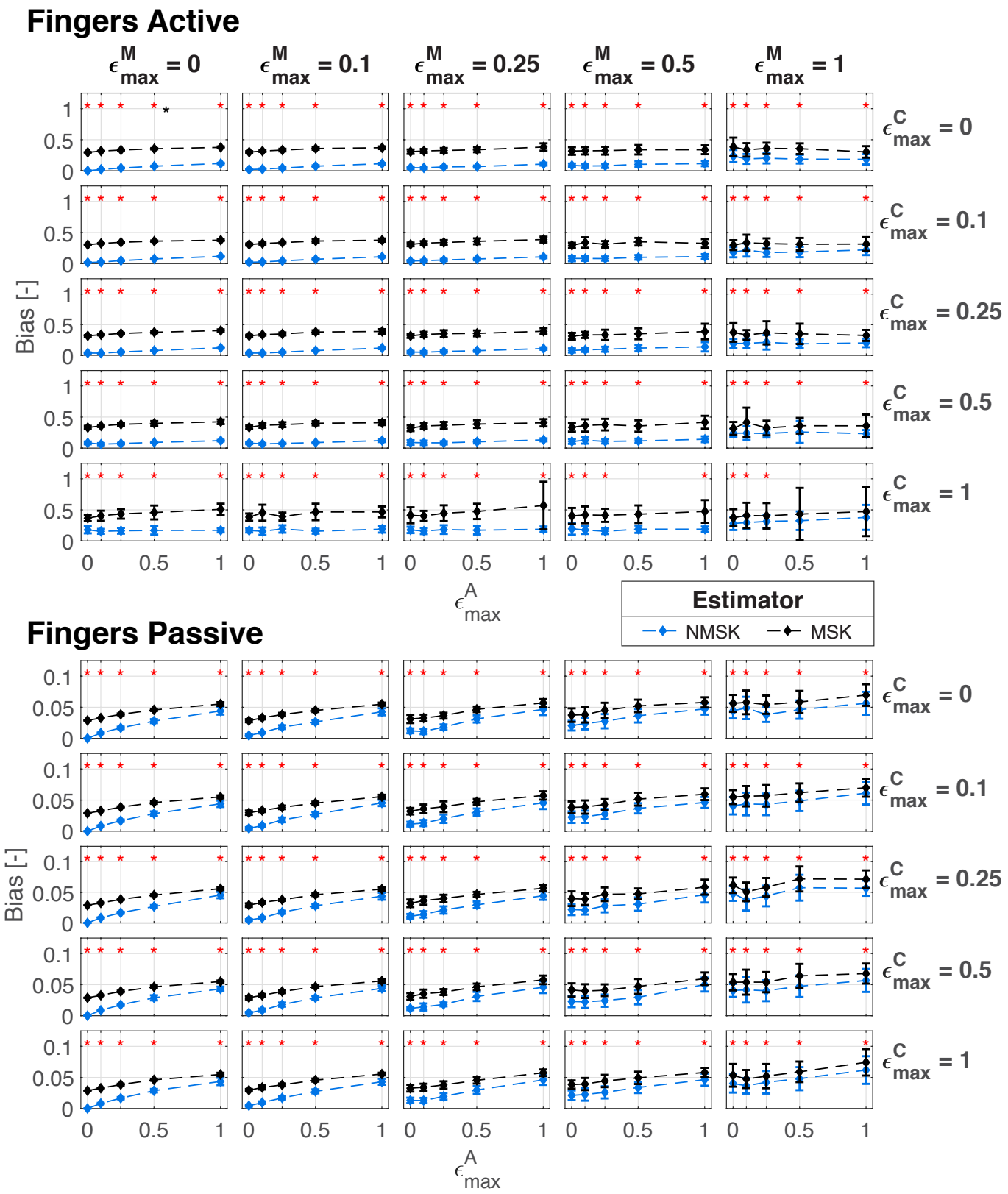

Fig. SM1. Values of metric $\bar{b}$ obtained for the NMSK estimator (in blue) and the MSK estimator (in black) when measurements are available only from the wrist muscles (MeasWrist) and for all levels of other factors. The top five rows include results obtained in presence of finger muscles (Ex=1), while the bottom five rows report the results obtained in the absence of finger muscles (Ex=0). In each subgroup rows encode levels of factor Me_2 (cross-talk), columns encode levels of factor Me_3 (measurement error), while the x-axis of each plot encodes levels of factor Ph (physiological variability). Asterisks are included in each condition if mean of the metric $\bar{b}$ obtained for the NMSK estimator was significantly lower than the one obtained for the MSK estimator. Significance level was set to be at 0.05 type I error rate.